Simple Method for RF Pulse Measurement Using Gradient Reversal

Vanessa L. Landes[1]* and Krishna S. Nayak[2]

Purpose: To develop and evaluate a simple method for measuring the envelope of small-tip radiofrequency (RF) excitation waveforms in MRI, without extra hardware or synchronization.

Theory and Methods: Gradient reversal approach to evaluate RF (GRATER) involves RF excitation with a constant gradient and reversal of that gradient during signal reception to acquire the time-reversed version of an RF envelope. An outer-volume suppression prepulse is used optionally to preselect a uniform volume. GRATER was evaluated in phantom and in vivo experiments. It was compared with the programmed waveform and the traditional pick-up coil method.

Results: In uniform phantom experiments, pick-up coil, GRATER, and outer-volume suppression + GRATER matched the programmed waveforms to less than 2.1%, less than 6.1%, and less than 2.4% normalized root mean square error, respectively, for real RF pulses with flip angle less than or equal to 30°, time-bandwidth product 2 to 8, and two to five excitation bands. For flip angles greater than 30°, GRATER measurement error increased as predicted by Bloch simulation. Fat-water phantom and in vivo experiments with outer-volume suppression + GRATER demonstrated less than 6.4% normalized root mean square error.

Conclusions: The GRATER sequence measures small-tip RF envelopes without extra hardware or synchronization in just over two times the RF duration. The sequence may be useful in prescan calibration and for measurement and precompensation of RF amplifier nonlinearity. **Magn Reson Med 79:2642–2651, 2018. © 2017 International Society for Magnetic Resonance in Medicine.**

Key words: RF fidelity; RF nonlinearity; predistortion correction

INTRODUCTION

Magnetic resonance imaging pulse sequences depend on accurate production of radiofrequency (RF) waveforms for precise excitation. Pulses with a high peak transmit RF magnetic field (B_1^+) and rapid fluctuations in their RF supply current can push the RF power amplifier to its limits, causing amplifier nonlinearity and incidental phase modulation (1–3). This leads to an incorrectly transmitted RF envelope and imperfect frequency profile, which can lead to undesirable effects in several advanced MRI applications (4). For example, distortions of multiband RF pulse envelopes can excite additional, unwanted side lobes and introduce errors in the separated, desired slices (2,5). Second, distortions of RF pulses used in hydrogen MR spectroscopy can lead to incorrect metabolite concentration quantification, as distorted water-suppression pulses saturate signal outside the expected bandwidth (6). Third, distortions of RF pulses used in hyperpolarized Xenon lung imaging can prevent excitation of Xenon inside vessels and tissues, and instead excite the 50-fold larger gas-phase magnetization pool (7). Because of increasing demand for higher fields, transmit array technology, and more complex excitation waveforms (8), accurate control of the RF field is now more necessary than ever.

Recent work has focused on improving the linearity of RF excitation by measuring the RF envelope to create a new waveform that corrects for expected nonlinearity. For example, Stang et al. (9,10) used a vector iterative predistortion method to iteratively detect and correct errors in RF transmit behavior in four parallel transmit channels, until the detected RF converged to the expected RF. Several groups have used forms of Cartesian feedback (namely, frequency-offset Cartesian feedback), to linearize coil current in multicoil transmit arrays through a negative feedback loop that corrects for transmit amplitude and phase error (8,11–13). Recently, Zhu et al. (2) presented a simple and elegant approach to correct for envelope distortion. This method uses an external pick-up coil placed in the scanner bore to measure RF, and processes the acquired data offline to determine the actualized envelope in relation to the programmed envelope. This method requires less hardware and processing, and has been demonstrated using single-channel transmit in a real RF pulse. The aforementioned methods can all minimize amplifier distortions, but at the cost of extra hardware, synchronization, and processing to measure actualized RF waveforms.

In this paper, we present a fast and simple method to measure RF waveforms without the need for extra hardware and synchronization. The proposed gradient-reversal approach to evaluate RF (GRATER) involves (i) excitation in the presence of a gradient and (ii) immediate signal acquisition in the presence of an inverted gradient along the same axis. The GRATER sequence relies on the scanner's intrinsic hardware and software to obtain the RF envelope by filtering and demodulating the RF signal. We demonstrate in phantoms and in vivo the ability of GRATER to quickly and easily capture RF waveforms, and compare measurements to the "gold standard" pick-up coil (PUC) method (2).

[1]Department of Biomedical Engineering, Viterbi School of Engineering, University of Southern California, Los Angles, California, USA.

[2]Ming Hsieh Department of Electrical Engineering, Viterbi School of Engineering, University of Southern California, Los Angles, California, USA.

Grant sponsor: National Institutes of Health; Grant number: R01-HL130494.

*Correspondence to: Vanessa Landes, M.S.E.E., Department of Biomedical Engineering, Viterbi School of Engineering, University of Southern California, 3740 McClintock Ave, EEB 400, Los Angeles, CA 90089-2564, USA. E-mail: vlandes@usc.edu.

A preliminary version of this work was presented in the Proceedings of 25th Annual Meeting of ISMRM, Honolulu, Hawaii, 2017, Abstract 78.

Received 10 May 2017; revised 21 August 2017; accepted 23 August 2017

DOI 10.1002/mrm.26920

Published online 14 September 2017 in Wiley Online Library (wileyonlinelibrary.com).

© 2017 International Society for Magnetic Resonance in Medicine

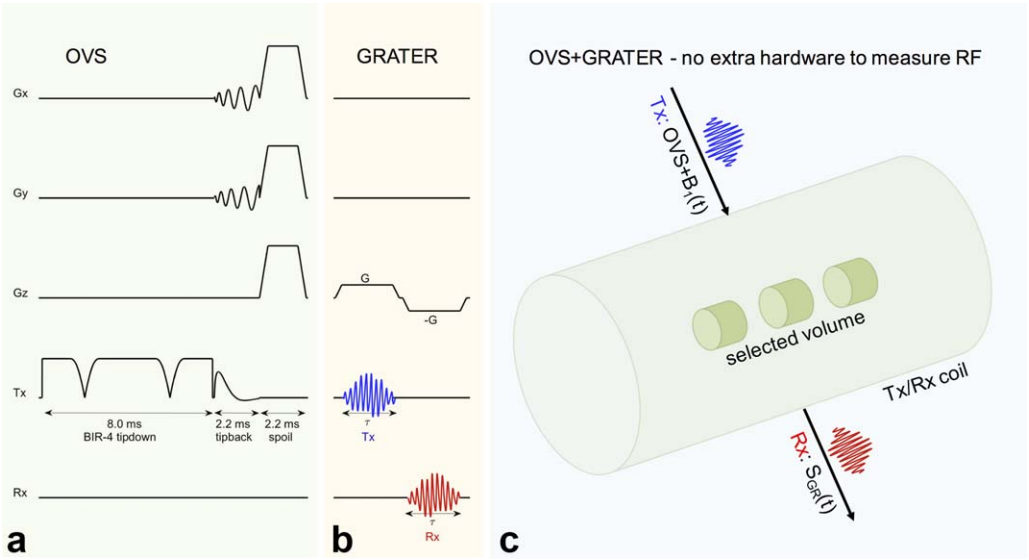

FIG. 1. The GRATER RF measurement consists of an optional (**a**) OVS prepulse and GRATER (**b**) with a simulated asymmetric RF pulse $B_1(t)$. The OVS prepulse (14) consists of a $+90^\circ$ BIR-4 tip-down, a -90° spiral tip-back pulse, and a gradient spoiler. The GRATER measurement consists of $B_1(t)$ in the presence of a constant gradient followed by signal acquisition in the presence of the same gradient, inverted. The received GRATER signal $S_{GR}(t)$ (red) is a time-reversed version of $B_1(t)$ (blue). **c**: The OVS and a slice-selective $B_1(t)$ excite volume with a single coil. $S_{GR}(t)$ is then acquired with the same coil.

THEORY

Figure 1 shows the GRATER pulse sequence for RF measurement with an optional outer volume suppression (OVS) prepulse (14). A constant gradient used during RF excitation is inverted during signal reception to acquire a time-reversed version of the RF pulse; the rationale follows.

Radiofrequency Excitation With Constant Gradient

Assuming a uniform object along the axis of an applied gradient and the small tip-angle approximation, the transverse magnetization $M(\tau, r)$ can be described at time τ after the RF pulse is played to select slice z. Here, $M(\tau, r)$ is proportional to the phase accumulated over the duration of the gradient with amplitude G to select slice z (i.e., $\omega(G,r) = \gamma Gz$), multiplied by the inverse Fourier transform of the angular frequency $\omega_1(s)$ at frequency $\omega(G,r)$ (see Eq. [1]):

$$M(\tau, r) \propto e^{-iw(G,r)\tau} \int_{s=0}^{\tau} e^{iw(G,r)s} \omega_1(s) ds \qquad [1]$$

The angular frequency $\omega_1(s)$ is a function of the Larmor frequency γ and the RF pulse $B_1(s)$, (i.e., $\omega_1(s) = \gamma B_1(s)$).

Signal Reception With Inverted Gradient

Using the small-tip approximation, GRATER signal is defined as $S_{GR}(t)$, where $t = 0$ corresponds to the beginning of the readout gradient with amplitude $-G$. Here, $S_{GR}(t)$ is proportional to the inverse Fourier transform of the magnetization at the frequency that corresponds to phase accrual during the readout gradient $-\omega(G, r) = \gamma(-G)z$. Phase terms $\Delta\omega(r)$ and $R_2^*(r)$ are added to account for off-resonance and transverse-relaxation rates, respectively (see Eq. [2]):

$$S_{GR}(t) \propto \int_x \int_y \int_z M(\tau, r) e^{-i(-\omega(G,r))t} e^{-i\Delta\omega(r)t} e^{-R_2^*(r)t} dz dy dz \qquad [2]$$

Assuming the object is uniform in x and y, off-resonance is minimal ($\Delta\omega(r) \approx 0$), and R_2^* effects are minimal ($R_2^*(r) \approx 0$), Equation [2] can be simplified to

$$S_{GR}(t) \propto \int_z M(\tau, r) e^{-i(-\omega(G,r))t} dz \qquad [3]$$

The GRATER Signal

Inserting Equation [1] into Equation [3], terms can be grouped such that the GRATER signal is proportional to the integral of the RF pulse with respect to s, multiplied by integrals of exponential terms with respect to s and z. These exponential terms can be regrouped and Fourier-transformed with respect to z to obtain a time-reversed, time-shifted impulse function. Finally, the sifting property can be applied to the integral of the product of the RF pulse and impulse function, to obtain an expression for the GRATER signal $S_{GR}(t)$ in terms of the RF pulse $B_1(t)$ and readout time τ (also slice-select time), as follows:

$$S_{GR}(t) \propto B_1(\tau - t) \qquad [4]$$

From Equation [4] it can be seen that $S_{GR}(t)$ is proportional to a time-reversed version of the RF pulse. Therefore, the signal $S_{GR}(t)$ can be used to measure the RF waveform under the assumptions stated previously.

For in vivo applications, we anticipate that a sufficiently large homogenous region can be found such that an OVS pulse can be used to eliminate signal from neighboring regions, allowing for a reasonable RF measurement to be made in vivo. The OVS pulse shown in Figure 1 is the

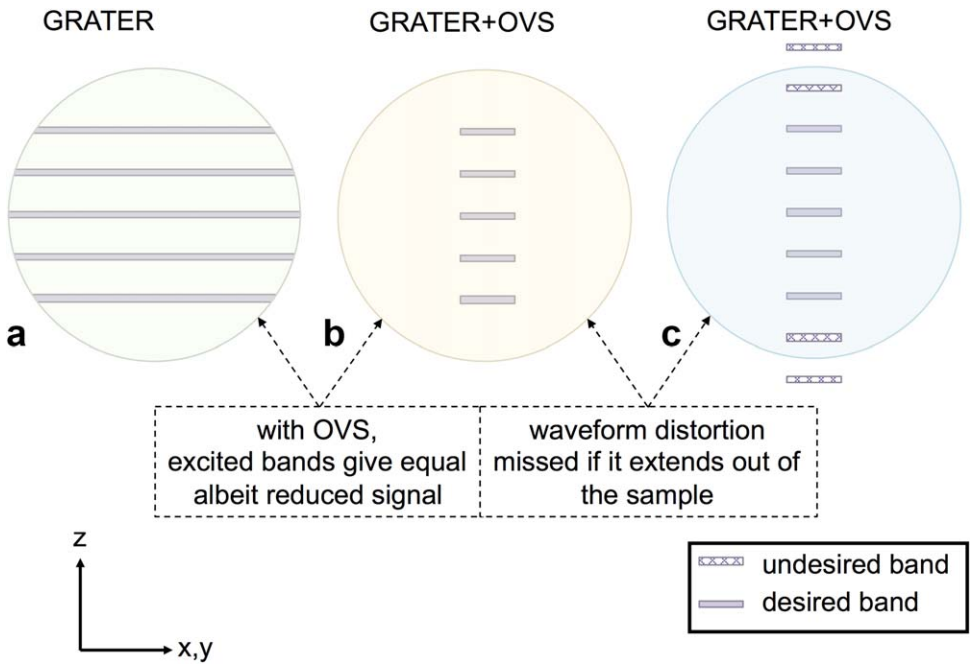

FIG. 2. Cartoon of excited slices from a five-band SMS RF pulse in a spherical phantom. The Fourier transform of $S_{GR}(t)$ gives a slice profile measurement in the small tip angle regime. **a**: If a GRATER measurement is obtained, artifacts will result from unequal signal contribution from each band (purple). **b**: If an OVS+GRATER measurement is taken, each band will contribute equal signal, but the signal-to-noise ratio will be lower. **c**: If waveform distortion is present, undesired bands can become excited (purple, hashed) and must be contained within the imaging volume to be detected.

design by Smith and Nayak (14), and includes a B_1-insensitive, nonselective tip-down followed by a cylindrical tip-up pulse. This suppresses signal outside of a cylinder with a diameter of 5 cm. In addition, the GRATER pulse sequence is shown in Figure 1. Note that the Fourier transform of $S_{GR}(t)$ gives a slice profile measurement in the small tip angle regime. Therefore, simultaneous multislice (SMS) pulses must be excited so that each slice contributes equal signal for an accurate GRATER measurement. In addition, any spurious sidebands must be within the sample volume to be detected by the GRATER method, as illustrated in Figure 2.

METHODS

Experiments were performed on a GE HD23 3T scanner (GE Healthcare, Little Chalfont, United Kingdom) using the body coil. The number of samples in the GRATER waveform was either matched to the programmed waveform or doubled by halving the GRATER readout gradient amplitude (RGA) and extending the readout duration. This allowed for easy comparison of measured versus expected (programmed) waveforms. Echo times were minimized to mitigate R_2^* effects. The RF waveforms were simultaneously measured using GRATER and an external pick-up coil, then adjusted as described in subsequent subsections.

Accuracy of GRATER was explored under near-ideal and nonideal conditions. To explore GRATER and OVS+GRATER under ideal conditions, experiments were performed on a variety of small flip-angle pulses in a uniform sphere phantom. Accuracy of the OVS+GRATER measurements was determined for different numbers of averages. The GRATER adjustment parameters were compared for waveforms acquired on the same day.

To explore GRATER under nonideal conditions, GRATER was first evaluated with large flip angles in a uniform sphere phantom and compared with Bloch simulation of GRATER waveforms. Second, GRATER was evaluated in nonuniform imaging volumes using GRATER and OVS+GRATER measurements in a fat-water (FW) phantom and in vivo.

The PUC measurements were considered the "gold standard" measurement method, and were compared with the GRATER measurement method. Normalized root mean square error (NRMSE) was calculated between programmed and measured waveforms. Raw GRATER data, raw PUC data, code to adjust measured waveforms, and code to perform the Bloch simulations of GRATER measurements are available at https://github.com/usc-mrel/GRATER; Release v1.2: https://doi.org/10.5281/zenodo.831849 (15).

GRATER Measurements

If the number of points in the measured GRATER waveform $S_{GR}(t)$ was twice that of the programmed waveform $S_{PW}(t)$ by halving RGA and extending the readout duration, then $S_{GR}(t)$ was first decimated with a Chebyshev type 1 IIR filter of order 12.

Measured $S_{GR}(t)$ were adjusted for a scale factor A, average relaxation rate R_2^*., average off-resonance Δw, initial-phase angle ϕ, and subsample time-shifts t_0 by solving a bounded minimum-norm least squares (MNLS) problem. $S_{PW}(t)$ was used as a reference, assuming that RF amplifier distortion is not present and thus not concealed. A captures proton density, transmit efficiency, and receiver gain.

The GRATER waveform was modeled as a distorted, time-reversed version of the programmed waveform as follows:

$$S_{GR}(t) \approx Ae^{-R_2^* t}e^{-i(\Delta\omega t+\phi)}S_{PW}(\tau - t - t_0) \quad [5]$$

The adjustment parameters were estimated according to

$$P \in \{A, R_2^*, \Delta\omega, \phi, t_0\} \quad [6]$$

Table 1
Summary of RF Pulse Parameters Used in a Uniform Sphere, FW Phantom, and In Vivo Experiments

Experiment	No. of bands	Duration (ms)	TBW	Bandwidth per band (Hz)	FA (°)	Slice center(s) (cm)	Slice thickness (cm)
Uniform sphere	2	2	2:2:8	TBW/2e-3	30	±2.5	1
(ideal conditions)	3	2	2:2:8	TBW/2e-3	20	0, ± 3.3	1
	4	2	2:2:8	TBW/2e-3	15	±1.25, ± 3.75	1
	5	2	2:2:8	TBW/2e-3	12	0, ± 2.5, ± 5	1
Uniform sphere (large FA)	1	1.28	4	3125	5:5:90	0	1
FW and in vivo	2	1.28	4	3125	15	±2.5	1

$$P = \min_{P} \|F^{-1}\{F\{Ae^{-R_2^* t}e^{-i(\Delta\omega t+\phi)}S_{PW}(\tau - t - t_0)\}e^{-k_z t_0}\} - S_{GR}(t)\|_2^2 \quad [7]$$

Parameters were bounded to prevent unreasonable estimates as follows: $A > 0$, $0.2 < R_2^* < 1000\,1/s$, $-2\pi 600 < \Delta\omega < 2\pi 600$ rad/s, $-\pi < \phi < \pi$, and $-10 < t_0 < 10\,\mu s$. Initial values were $A = \max(abs(S_{GR}(t))/\max(abs\ (S_{PW}(t))$, $R_2^* = 1000\,1/s$, and $t_0 = 0\,\mu s$. Choosing a high initial R_2^* prevented finding local-minimum solutions of this parameter. Because $\Delta\omega$ and ϕ adjusted complex GRATER data and were more likely to produce local-minimum solutions, 10 equally spaced initial values were chosen for these two parameters , and parameters that gave lowest NRMSE were kept. The GRATER waveform was adjusted as $S_{GR,A}(t)$ as follows:

$$S_{GR,A}(t) = F^{-1}\{F\{1/A\, e^{R_2^* t}e^{i(\Delta\omega t+\phi)}S_{GR}(t)\}e^{k_z t_0}\} \quad [8]$$

The transmitted RF envelopes in this study were real, so the real part of the adjusted waveform was compared with the programmed waveform and PUC measurements. Previous approaches have noted that measurement followed by predistortion of the real RF pulse is a simple, sufficient way to reduce undesired higher harmonics (2), and the ultimate intended application of GRATER is for use with predistortion techniques.

Pick-up Coil Measurements

Pick-up coil measurements were demodulated and filtered similarly to the method described by Zhu et al. (2), with the following exceptions. First, the modulated RF data were bandpass-filtered to allow ±5 MHz around the center frequency. Second, the demodulated RF data were low-pass-filtered with a cut-off frequency of 200 KHz. Lowering the range of the bandpass filter and lowering the cutoff frequency of the low-pass filter reduced noise without compromising the shape of the measured waveform. Third, a bounded MNLS optimization problem was solved and corrected for amplitude, timing, and center frequency offsets. This problem was similar to the GRATER bounded MNLS problem, except that $R_2^* \approx 0$.

Radiofrequency Pulse Design

Table 1 provides the parameters of the RF pulses used in each experiment. Single-band RF pulses were generated in MATLAB using the function dzrf() from the rf_tools software package based on (16). The sampling period was 4 μs. Then, the single-band pulse was multiplied by a sum of complex exponentials, B(t), to create multiband pulses. The sum followed the form

$$B(t) = \sum\nolimits_i e^{i\omega(G,z_i)} \quad [9]$$

where z_i represents the slice location of an i-band pulse.

Near-Ideal Conditions

Measurements were made in a 27-cm-diameter uniform sphere with several multiband pulses to demonstrate GRATER in near-ideal conditions. The pulse parameters were 2-ms pulses; 500 points; and time bandwidth (TBW) = 2, 4, 6, or 8: two bands with flip angle (FA) = 30°, three bands with FA = 20°, four bands with FA = 15°, or five bands with FA = 12°.

To ensure each excited slice was contained within the 27-cm volume and measureable by GRATER, and to ensure that signal-producing volume came from the linear region of the gradients to avoid side-band amplitude weighting, pulses were designed to have slice centers within ±5 cm of the center of the phantom. Because the different slices in the uniform sphere phantom could contribute different signal, OVS+GRATER measurements were obtained and compared with GRATER measurements. To account for limited signal-to-noise ratio with a limited excited volume, multiple averages were obtained and NRMSE was calculated for measurements using averages of 2:2:64 GRATER measurements. The NRMSE for different averages was fitted according to $\%\ NRMSE = m/\sqrt{\#\ averages} + b$, where A represents the fitted error floor and B represents the rate of error decay.

To measure high frequencies in the GRATER-measured waveforms, the amplitude of the GRATER readout gradient was halved to effectively double the sampling period of the GRATER waveform. Results were compared with measurements obtained with a sampling period matched to the transmitted waveform.

To assess the consistency of MNLS-determined adjustment parameters, values were calibrated and compared for each pulse in GRATER measurements using matched RF sampling and transmit periods.

Nonideal Conditions: Large Flip Angles

The GRATER measurements and Bloch simulations of GRATER measurements were compared to evaluate GRATER outside the small-tip regime (17). To rule out

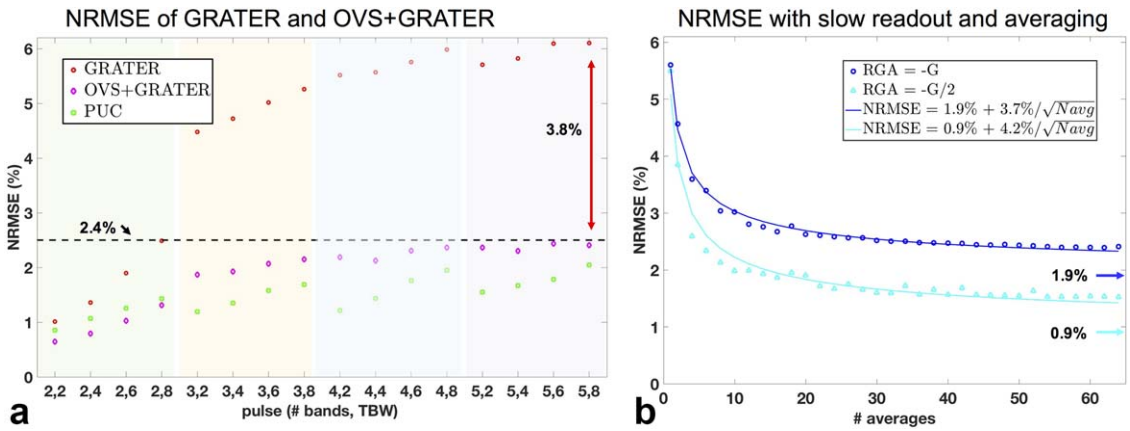

FIG. 3. The NRMSE of uniform sphere experiments for SMS pulses with different numbers of bands and TBW products. **a**: The NRMSE for 64 averaged GRATER and OVS+GRATER with RGA = − G, the negative excitation gradient amplitude. The GRATER NRMSE was higher with more slices and was reduced with OVS to less than or equal to 2.4% (black dashed line) by up to 3.8% (red arrow). The NRMSE in PUC was less than or equal to 2.1%. **b**: The NRMSE decreases with averaging of OVS+GRATER in a five-band, TBW = 8 pulse for RGA = − G. It decreases more and faster for RGA = − G/2. Data were fitted to $\%\ NRMSE = m/\sqrt{\#\ averages} + b$ (solid lines). Fitted error floors are shown (arrows).

error in GRATER measurements caused by sources other than large flip angles, a uniform sphere phantom was used. A real single-band (TBW = 4) RF pulse with flip angles ranging from 5 to 90° in 5° increments was measured. This simple pulse was used to isolate and identify the predictable errors in large flip-angle GRATER measurements from other sources of error.

Bloch simulations were performed using a sampling period of 4 μs, $T_1 = 2000$ ms, $T_2 = 200$ ms, gradient amplitude $G = 0.733983$ G/cm, and z-positions = 30 : 0.1 : 30 cm. Off-resonance was assumed to be negligible. After simulating RF excitation in the presence of a gradient, the magnetization was calculated every 4 μs for each z-position during a subsequently inverted gradient to simulate the GRATER measurement. Then, the final GRATER measurement was calculated as the one-dimensional temporal signal averaged over each z-position (i.e., the whole simulated imaging volume).

The GRATER measurements and Bloch simulations of GRATER measurements were adjusted by solving the bounded MNLS problem described previously with the programmed waveform, divided by its maximum amplitude, as reference. This scaling was done to emphasize errors in the shape of GRATER measurement and Bloch simulation of the measurement. To test the predictability of GRATER measurement error caused by deviations from the small-tip approximation, the NRMSEs between GRATER and simulations of GRATER measurements were compared.

Nonideal Conditions: Inhomogeneous Objects

To evaluate GRATER in inhomogeneous objects with high off-resonance, a FW phantom was used to compare RF measurements using (i) GRATER, (ii) OVS+GRATER, and (iii) the PUC method in regions containing (i) water only, (ii) fat only, and (iii) both fat and water. Measurements were made in a two-band, 1.28-ms, 320-point, TBW = 4 RF pulse with FA = 15°. The GRATER measurements were made without averaging and with matched sampling and transmit rates.

To demonstrate GRATER in an in vivo imaging volume, the same two-band pulse in the FW phantom experiments was measured using (i) GRATER, (ii) OVS+GRATER, and (iii) the PUC method in an axial brain slice above the ventricles in two healthy volunteers (male, ages 27 and 30). Each subject was screened, and each provided written informed consent with approval from the institutional review board.

RESULTS

Near-Ideal Conditions

The GRATER measurements were made in a variety of pulses using the uniform sphere phantom. The NRMSE of GRATER measurements increased for higher numbers of bands and TBW products (Fig. 3a). Higher error comes from unequal signal contribution from each excited band and is described in Figure 2. For example, the waveforms matched most closely in the two-band, TBW = 2 RF pulse, in which the GRATER versus programmed and PUC versus programmed waveforms had 1.1 and 0.9% NRMSE, respectively. The NRMSE was highest in the five-band, TBW = 8 RF pulse, in which the NRMSE between GRATER versus programmed and PUC versus programmed waveforms had 6.1 and 2.1% NRMSE, respectively. To lower the NRMSE in GRATER, two strategies were shown to be helpful: (i) averaging the OVS+GRATER measurements and (ii) lowering RGA and extending the readout duration to acquire more points in the GRATER-measured waveform.

Figure 3a shows lower NRMSE with 64 averaged OVS+GRATER measurements versus 64 averaged GRATER measurements. The biggest improvement was seen in the five-band, TBW = 8 RF pulse with 3.8% reduction in NRMSE from 6.1 2.4%. Over the 16 RF pulses with parameters provided in Table 2, the mean ± standard deviation of NRMSE was 4.4 ± 1.7% NRMSE for averaged GRATER measurements and 1.9 ± 0.60%

Table 2
Summary of Adjustment Parameters for GRATER Waveforms Without OVS or Averaging in Uniform Sphere Experiments in the Same Scan Session With the Same Prescan

No. of bands, TBW	A (a.u.)	R_2^* (1/s)	$\Delta\omega$ (rad/s)	ϕ (rad)	t_0(μs)
2, 2	.69	100	−0.0022	−0.15	−0.62
2, 4	.68	110	−0.0023	−0.15	−0.60
2, 6	.68	130	−0.0027	−0.13	−0.63
2, 8	.67	140	−0.0032	−0.11	−0.63
3, 2	.69	86	−0.0023	−0.15	−0.72
3, 4	.70	90	−0.0025	−0.14	−0.66
3, 6	.69	97	−0.0031	−0.11	−0.56
3, 8	.68	110	−0.0036	−0.09	−0.60
4, 2	.68	110	−0.0025	−0.13	−0.63
4, 4	.68	110	−0.0030	−0.11	−0.57
4, 6	.67	130	−0.0032	−0.10	−0.56
4, 8	.66	140	−0.0030	−0.12	−0.67
5, 2	.69	100	−0.0025	−0.12	−0.66
5, 4	.68	100	−0.0024	−0.14	−0.66
5, 6	.68	120	−0.0029	−0.12	−0.62
5, 8	.66	140	−0.0060	−0.01	−0.68
Mean	.68	110	0.0030	−0.12	−0.63
CV (%)	2.8%	16.3%	30%	28%	7.1%

Note: Parameters were solved with a bounded MNLS problem for pulses with different numbers of bands (# bands) and TBW products. The bottom two rows show the mean and CV for each parameter value. The CV was low for A. Calculated R_2^* values were larger than the phantom's R_2 of 33 1/s. With a good shim, $\Delta\omega \approx 0$ in all cases. $\Delta\phi$ varied from scan to scan. t_0 was consistent to within 7.1% CV.

NRMSE for averaged OVS+GRATER measurements. Furthermore, the clear trend of higher NRMSE for higher numbers of bands and higher TBW product in GRATER measurements is not seen in OVS+GRATER measurements. For comparison, the mean ± standard deviation was 1.5 ± 0.30% NRMSE with the PUC method.

Figure 3b shows improvement with lowered RGA as a function of the number of averaged OVS+GRATER measurements in the five-band, TBW = 8 RF pulse. Over 64 averages, the NRMSE decreased from 2.4% for RGA = − G to 1.5% NRMSE for RGA = − G/2. After fitting the curves of NRMSE versus the number of averages to the equation $\%\ NRMSE = m/\sqrt{\#\ averages} + b$, the fitted error floor b decreased from 1.9 to 0.9% NRMSE for RGA = − G and RGA = − G/2, respectively. Furthermore, the fitted rate of error decay m increased from 3.7 to 4.2% NRMSE for RGA = − G and RGA = − G/2, respectively.

Figure 4 visualizes the best-measured improvement of the five-band, TBW = 8 RF pulse by combining both strategies of 64 averages of OVS+GRATER combined with RGA = −G/2 to lower NRMSE. The GRATER measurements without OVS, PUC measurements, and the programmed waveform are shown for comparison. Figure 4a shows that the errors in GRATER measurement are most prominent in the high-frequency peaks and valleys of the RF lobes, as a result of the unequal signal contribution for each of the five bands. This error is greatly reduced with OVS. The difference between the measured and programmed waveform are also shown in Figure 4b. There is clear structure to the difference waveform of GRATER without OVS. This structure is reduced with OVS; however, the cause of the remaining structure is unresolved.

Table 2 lists the consistency of MNLS-determined adjustment parameters determined for each of the 16 SMS RF pulses in GRATER measurements using matched RF sampling and transmit periods, all acquired during the same scan session. Prescan was run once for these experiments, and the coefficient of variation (CV) was low for A. The calculated R_2^* values were all larger than the phantom's true R_2 of 33 1/s. With a good shim, $\Delta\omega \approx 0$ in all cases. t_0 was consistent to within 7.1% CV. Of the adjustment parameters, ϕ varied the most from scan to scan.

Nonideal Conditions: High Flip Angles

Figure 5 shows results of high flip-angle experiments in Bloch simulations of GRATER measurements and

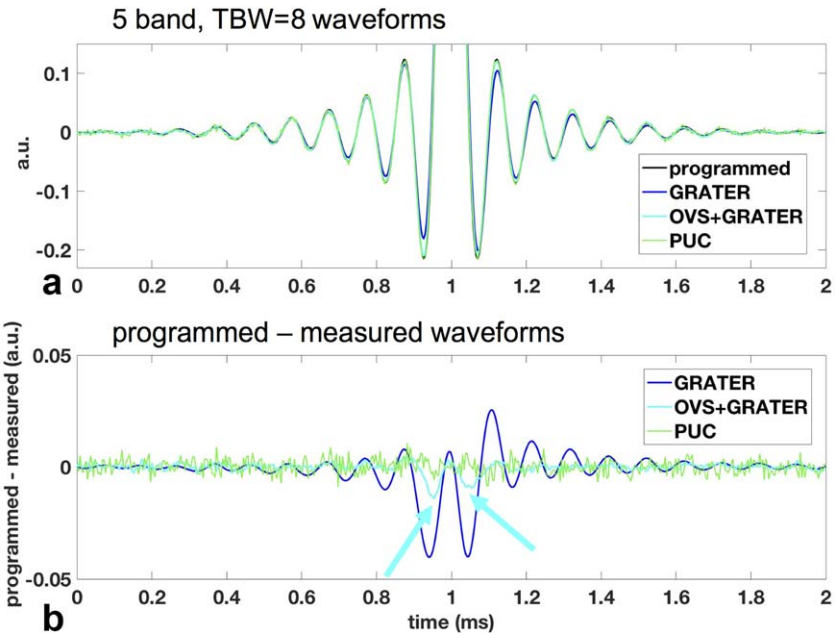

FIG. 4. The GRATER measurement using a five-band, TBW = 8 RF pulse in a uniform sphere. **a**: A programmed RF pulse was measured using PUC (black), and 64 averages with RGA = − G/2 of GRATER (blue) and OVS+GRATER (cyan). The zoomed-in lobes in the GRATER waveform show error from unequally excited bands and can be seen more clearly with the difference between waveforms in (**b**). Compared with programmed waveforms and PUC, GRATER matches with less than 5.7% NRMSE, and less than 1.5% with OVS+GRATER. There is structure in the difference between programmed and OVS+GRATER measurements (arrows), and the source of this error is unresolved.

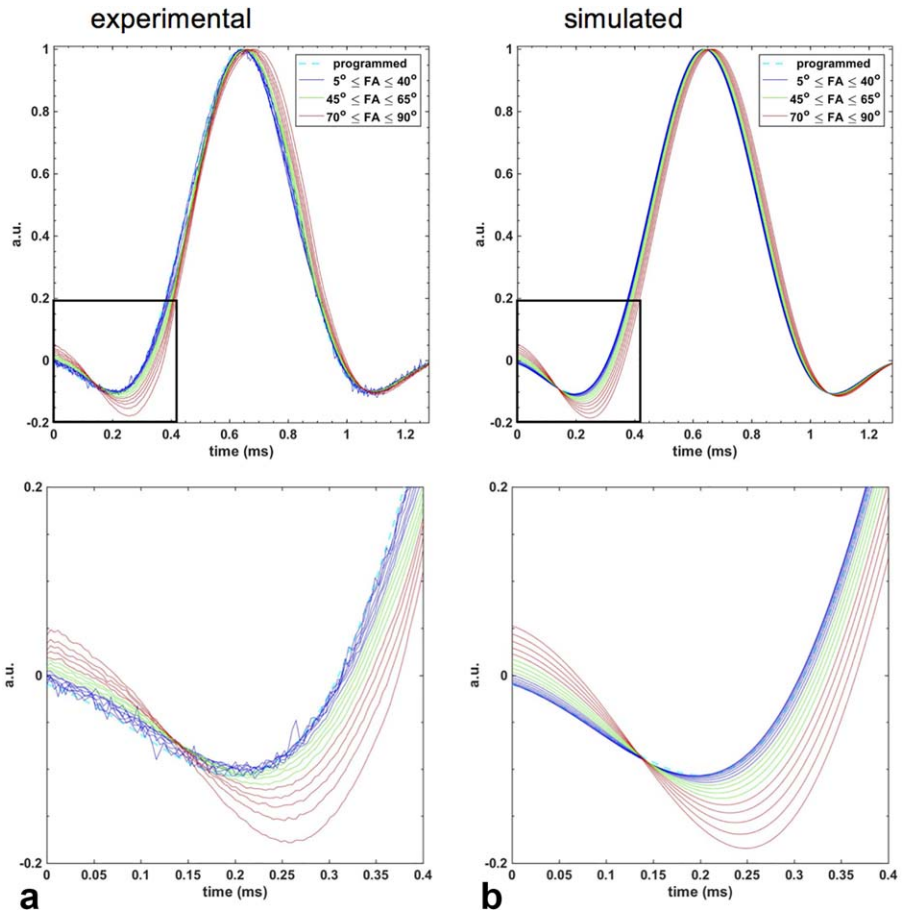

FIG. 5. Experimental GRATER measurements (**a**) and Bloch simulations (**b**) of GRATER measurements of a single-band RF pulse in a uniform sphere phantom with flip angles in 5° increments from 5° to 90°, adjusted so that the programmed pulse, divided by its maximum amplitude, was used as reference. Measurements with a small flip angle ($5° \leq FA \leq 40°$) are shown in blue, in-between flip angles ($45° \leq FA \leq 65°$) in green, and large flip angles ($70° \leq FA \leq 90°$) in red. The NRMSE between GRATER measurements and simulations for a given flip angle was less than 2.4%. Top row shows the total waveform. The boxed-off portions are shown in the bottom row, zoomed.

experimental GRATER measurements, plotted over the same range to emphasize the shape of the GRATER measurement compared with the programmed waveform. Both plots show the programmed RF pulse as a reference in dashed cyan. The RF pulses with flip angles of less than or equal to 40° are plotted in blue, 45 to 65° in green, and greater than or equal to 70° in red. This demonstrates that GRATER measurement error increases for increasing flip angles. The GRATER-measured and Bloch-simulated measurements matched to less than 2.4% for each flip angle pair. This implies that GRATER measurement error occurred in a patterned, predictable way.

Nonideal Conditions: Inhomogeneous Objects

Figure 6 compares RF measurements of a FW phantom using GRATER, OVS+GRATER, and the PUC method to evaluate GRATER in inhomogeneous objects with high off-resonance. The imaging slice is shown without OVS in Figure 6a, where F and W represent fat and water, respectively. The imaging slice is shown with OVS in Figure 6b to demonstrate the ability of the OVS pulse to select a 5-cm-diameter region. Figure 6c shows the programmed 1.28-ms, 320-point, two-band, and TBW = 4 RF pulse in black, the PUC method in red, and the OVS+GRATER measurement in dashed black.

Figure 7 compares RF measurements in two healthy subjects using GRATER, OVS+GRATER, and the PUC method. Figure 7a shows that an axial slice above the ventricles was excited in the brain for GRATER measurements. Figure 7b shows an excited 5-cm cylinder in the center of the axial slice to avoid off-resonance at the brain–skull interface. Figure 7c shows measurements of a 1.28-ms, 320-point, two-band, TBW = 4 RF pulse against the programmed waveform. The PUC, GRATER, and programmed waveform all matched to less than 3.0% difference. The PUC and OVS+GRATER waveform matched to less than 4.5%.

Figure 8 summarizes NRMSE values for FW phantom and in vivo experiments. There was less than 1.5% difference in PUC versus programmed measurements. The PUC versus GRATER measurements differed by 58% in the fat+water of the FW phantom, and less than 12% NRMSE in all other cases. The PUC versus OVS+GRATER measurements differed by less than 6.4% NRMSE in the water of the FW phantom and in the brain. Although OVS+GRATER versus PUC had lower NRMSE than GRATER versus PUC in the FW phantom, an OVS prepulse increased the NRMSE of GRATER measurements in the brain. The mean NRMSE in inhomogeneous objects of PUC versus programmed was $1.2 \pm 0.2\%$, PUC versus GRATER was $17 \pm 25\%$, and PUC versus OVS+GRATER was $5.1 \pm 1.1\%$.

DISCUSSION

This study has successfully demonstrated measurement in a variety of small-tip RF waveforms to within less

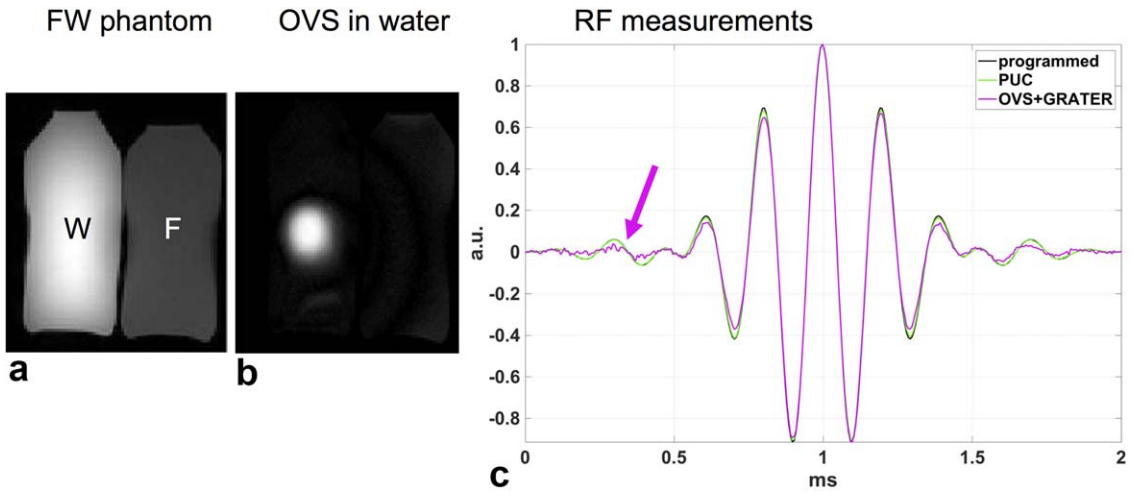

FIG. 6. The GRATER measurement in a fat-water phantom. The imaging slice without (**a**) and with (**b**) OVS (F, fat; W, water). **c**: A programmed 1.28-ms, 320-point, two-band, and TBW = 4 RF pulse (black) was measured using PUC (green) and OVS+GRATER (magenta). The NRMSE was less than 6.4% between programmed, PUC, and OVS+GRATER measurements. The OVS+GRATER measurement is time-reversed (see Eq. [2]); noise increases toward the end of the measurement (arrow).

than 2.4% NRMSE using averaged OVS+GRATER measurements in uniform volumes. It has also demonstrated that acquiring more points in the measured waveform further lowered NRMSE. In nonuniform volumes, an NRMSE of less than 6.4% was achieved using OVS+GRATER without averaging. A variety of methods to further improve the GRATER technique form the core of this discussion.

Normalized root mean square error was used in this study as a generic metric to describe error between any RF waveforms or measurements, and to establish GRATER's accuracy under different conditions. However, NMRSE may not be the ideal metric for RF pulse correction, and application-specific metrics could be more useful. For example, spurious side-lobe excitation may be more appropriate to evaluate SMS-RF pulses, or stop-band suppression for spectral-editing RF pulses. Regardless of the specific metric, the accuracy of GRATER would have to match or surpass the accuracy of the PUC method to be a successful measurement technique and detect subtle RF amplifier nonlinearity. Therefore, it is important to acknowledge GRATER's successes and investigate ways to overcome its current limitations.

The GRATER and PUC measurements matched very closely in the uniform sphere phantom for small flip angle pulses with two bands, such as the 2-μs, two-band, TBW = 2 RF pulse. However, error in GRATER measurements increased in RF pulses with higher numbers of bands as a result of the unequal signal coming from each excited slice. These RF pulses may have also contained an error that GRATER was unable to fully capture at the current sampling period of 4 μs (i.e., readout bandwidth of 125 kHz). This limitation is best seen in the 2-μs, five-band, TBW = 8 RF pulse, in which the GRATER error is

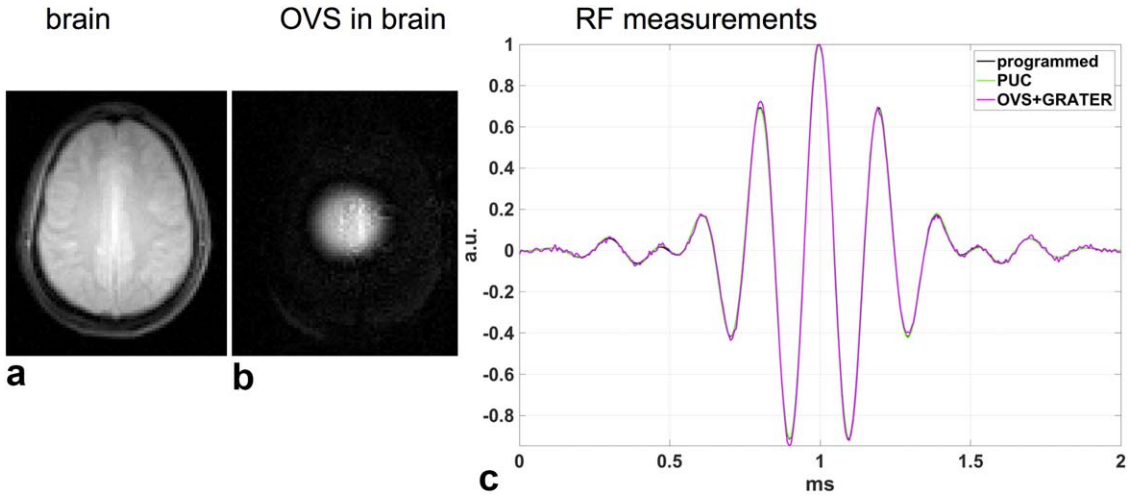

FIG. 7. The GRATER measurement in the brain of one volunteer. The imaging slice without (**a**) and with (**b**) OVS. An imaging slice was chosen superior to the ventricles. Measurements of a 1.28-ms, 320-point, two-band, and TBW = 4 RF pulse using (i) the PUC method and (ii) the OVS+GRATER method are plotted against the programmed waveform in (**c**). The PUC, GRATER, and programmed waveforms match to less than 3.0% NRMSE. The OVS+GRATER versus PUC methods had less than 4.5% NRMSE.

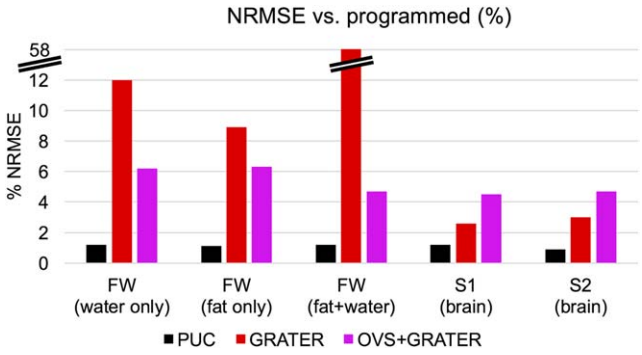

FIG. 8. The NRMSE of experiments in nonuniform samples: the FW phantom, subject 1 (S1), and subject 2 (S2). The NRMSE was calculated between the PUC method and (i) the programmed waveform, (ii) the measured GRATER waveform, and (iii) the measured OVS+GRATER waveform. The PUC versus GRATER methods had 58% NRSME in fat+water. The OVS improved the accuracy of GRATER to 6.4%. The PUC versus programmed waveforms had less than 1.5% NRMSE.

highest on either side of the main lobe. The NRMSE was reduced by (i) using an OVS prepulse to obtain equal signal from each slice, (ii) averaging to overcome the reduced signal-to-noise ratio in each slice as a result of OVS, and (iii) lowering the amplitude and extending the duration of the readout gradient to traverse excitation k-space more slowly and acquire more points in the GRATER-measured waveform. Although the error has been reduced, the difference between the programmed and best-measured waveform still has structure. This could be because of the need for an even faster sampling period through a further lowered and extended readout gradient or increased receive sampling rate. This could also be explained by imperfect OVS pulse performance.

For measurements in inhomogeneous objects, recall that GRATER is a proton density–weighted measurement. For this reason, GRATER measurements will be best in areas where the excited region has as uniform proton density as possible. Therefore, error measurement in the chosen slices could be the result of signal coming from inhomogeneous tissues (i.e., fine structures in the brain). Although one OVS prepulse is demonstrated in this study (14), GRATER in different situations may benefit from the selection of different size volumes. Spectral prepulses could also be used, such as a water saturation prepulse followed by GRATER measurement in subcutaneous fat near a receive coil.

The OVS+GRATER measurement is time-reversed and was clearly emphasized in GRATER measurements with fast signal attenuation in the fat-water phantom, and is not likely to be resolved with averaging. Noise in the end of the measurement became more prominent. To resolve this error, different sections of the RF pulse could be recorded in successive GRATER measurements, then combined to produce a complete measurement. More signal remained from the RF measurement toward the end of the OVS+GRATER measurement in the brain than in the FW phantom. This indicates different R_2^* of the two volumes.

Compared with GRATER, OVS+GRATER more accurately captured RF waveforms in the FW phantom, but not in the brain. Gains in excited volume uniformity with an OVS prepulse were not enough to offset the decrease in signal-to-noise ratio caused by limiting the region of excited tissue with an OVS pulse. Although OVS+GRATER measurement averaging is a viable option, as demonstrated in the uniform sphere experiments, adjusting the GRATER excitation and readout gradient amplitudes may further reduce NRMSE. If the amplitudes are decreased, slice thickness and signal-to-noise ratio could be increased in volumes with low signal. However, this may decrease excited sample uniformity and increase through-slice dephasing. If the amplitudes are increased, errors caused by erroneous phase in SMS bands as a result of B_0 variation will be mitigated by making the excited volume small in the z-direction. In addition, potential amplitude weighting of side bands caused by nonlinearity in the selection gradient, similar to the pile-up artifacts seen in scans with nonlinear frequency position mapping, could be reduced.

The waveforms in this study were designed to establish and evaluate the feasibility of the GRATER method in phantoms and in vivo, and were not designed to push the RF amplifier into its nonlinear regime. If one is using GRATER to correct for RF amplifier nonlinearity, it is of concern that adjustments relative to the ideal programmed waveform may conceal waveform distortions. The consistency of adjustment parameters has been demonstrated from scan to scan, and this decreases concern. Therefore, GRATER may be made more efficient by reusing parameters from scan to scan.

Despite all of this, comparing or even replacing MNLS-determined adjustment parameters with sequence-based measurements will be useful in the future. For example, simple pulse sequences can be used to measure or correct for R_2^*, $\Delta\omega$, and t_0 instead of estimating them in a bounded MNLS problem. More specifically, R_2^*, $\Delta\omega$, and ϕ can be measured with an FID. In addition, $\Delta\omega$ can be measured and corrected for using a B_0 mapping technique, and t_0 between the GRATER measurement and PUC waveform can corrected with gradient delays. Finally, to reduce noise in GRATER using averaging while simultaneously measuring R_2^*, the GRATER read-out waveform can be repeatedly inverted and data can be acquired during each inversion to acquire multiple GRATER measurements. These measurements will be weighted with the R_2^* relaxation rate. Timing errors would likely occur with reverse polarity readouts; therefore, other adjustment parameters, especially t_0, would have to be calculated for each readout.

Finally, GRATER may be useful for predistortion with large imaging volumes and small flip-angle RF pulses, such as short SMS pulses with a high number of bands that push the RF amplifier into its nonlinear region. For large flip-angle pulses, it has been demonstrated that GRATER measurement error and Bloch simulation of GRATER measurement error increased as the flip angle increased from 30° to 90°, and that GRATER measurement error was predictable by simulation. Although GRATER's potential for RF measurement has been demonstrated, its applicability for use with predistortion

techniques is a topic of future work, both in small and large flip-angle RF pulses.

CONCLUSIONS

In conclusion, GRATER is a promising new technique for RF envelope measurement. Compared with the traditional pick-up coil technique, GRATER is fast, and requires no hardware and no synchronization. The GRATER technique measured the two-band TBW = 2 RF pulses accurately compared with the PUC method under ideal conditions. Including OVS prepulses, averaging measurements, and acquiring more points in the GRATER waveform were shown to increase accuracy for pulses with higher numbers of bands and TBW. In large flip angles, GRATER measurement error occurs in a way that is predictable by Bloch simulation. In nonuniform volumes, an OVS prepulse may select a uniform region and improve GRATER measurements. The GRATER technique may be useful in prescan calibration, and for measurement and precompensation of RF amplifier nonlinearity.

ACKNOWLEDGMENTS

We thank Kangrong Zhu for helpful discussions about RF system imperfections, and Dwight Nishimura for inspiring this method through homework question 6.4 in his textbook (18).

REFERENCES

1. Chan F, Pauly J, Macovski A. Effects of RF amplifier distortion on selective excitation and their correction by prewarping. Magn Reson Med 1992;23:224–238.
2. Zhu K, Dougherty RF, Middione MJ, Wu H, Scott G, Pauly JM, Kerr AB. RF amplifier nonlinearity correction for multiband RF pulses. In Proceedings of the 23rd Annual Meeting of ISMRM, Toronto, Canada, 2015. p. 1830.
3. Setsompop K, Gagoski BA, Polimeni JR, Witzel T, Wedeen VJ, Wald LL. Blipped-controlled aliasing in parallel imaging for simultaneous multislice echo planar imaging with reduced g-factor penalty. Magn Reson Med 2012;67:1210–1224.
4. Razavi B. RF microelectronics. Upper Saddle River, NJ: Prentice-Hall; 2013. pp 11–22.
5. Cunningham CH, Wood ML. Method for improved multiband excitation profiles using the Shinnar-Le Roux transform. Magn Reson Med 1999;42:577–584.
6. Kreis R. Issues of spectral quality in clinical 1H-magnetic resonance spectroscopy and a gallery of artifacts. NMR Biomed 2004;17:361–381.
7. Kaushik SS, Freeman MS, Cleveland ZI, et al. Probing the regional distribution of pulmonary gas exchange through single-breath gas- and dissolved-phase 129Xe MR imaging. J Appl Physiol 2013;115: 850–860.
8. Zanchi MG, Stang P, Kerr A, Pauly JM, Scott GC. Frequency-offset cartesian feedback for MRI power amplifier linearization. IEEE Trans Med Imaging 2011;30:512–522.
9. Stang P, Kerr AB, Grissom W, Pauly JM, Scott GC. Vector iterative pre-distortion: an auto-calibration method for transmit arrays. In Proceedings of the 17th Annual Meeting of ISMRM, Honolulu, Hawaii, USA, 2009. p. 395.
10. Stang P, Zanchi M, Grissom WA, Kerr A, Pauly JM, Scott GC. RF sensor considerations for input predistortion correction of transmit arrays. In Proceedings of the 18th Annual Meeting of ISMRM, Stockholm, Sweden, 2010. p. 44.
11. Hoult DI, Kolansky G, Kripiakevich D, King SB. The NMR multitransmit phased array: a Cartesian feedback approach. J Magn Reson 2004;171:64–70.
12. Zanchi M, Pauly J, Scott G. Frequency offset Cartesian feedback control system for MRI power amplifier. In Proceedings of the 17th Annual Meeting of ISMRM, Honolulu, Hawaii, USA, 2009. p. 398.
13. Stang PP, Zanchi MG, Kerr A, Pauly JM, Scott GC. Active coil decoupling by impedance synthesis using frequency-offset Cartesian feedback. In Proceedings of the 19th Annual Meeting of ISMRM, Montreal, Canada, 2011. p. 332.
14. Smith TB, Nayak KS. Reduced field of view MRI with rapid, B 1-robust outer volume suppression. Magn Reson Med 2012;67:1316–1323.
15. Landes V, Nayak KS. usc-mrel/GRATER: release v1.2. Zenodo 2017. https://doi.org/10.5281/zenodo.846434. Accessed August 21, 2017.
16. Pauly J, Nishimura D, Macovski A, Roux P Le. Parameter relations for the Shinnar-Le Roux selective excitation pulse design algorithm. IEEE Trans Med Imaging 1991;10:53–65.
17. Hargreaves B. Bloch simulation equation. http://www.mrsrl.stanford.edu/~brian/bloch. Accessed April 15, 2017.
18. Nishimura D. Principles of magnetic resonance imaging, 1st edition. Raleigh, NC: Lulu; 1996. pp 119–132.